(Preprint) AAS 20-641

SAFE TRAJECTORY DESIGN FOR CLOSE PROXIMITY OPERATIONS

Gabriella Gaias* **and Marco Lovera†**

This work addresses the design of safe relative trajectories to enable satellite close proximity operations for a variety of multi-satellite missions. With regard to active debris removal and on-orbit servicing applications, first the key aspects driving the different operational concepts are identified. Afterwards, these are translated into requirements for the trajectory design, carried out in the relative orbital elements framework. As a result, the paper provides guidelines and methodologies to compute relative trajectories applicable to different mission scenarios, considering the optimality in the location of the maneuvers and safety considerations.

INTRODUCTION

A new generation of space missions capable to perform autonomous close proximity operations (CPOs) with respect to another satellite are currently under development. The novelty aspect consists in the fact that the target spacecraft is not designed *ad hoc* to support interaction with another satellite or may not be prepared to undergo and aid the interaction phase. Examples are active debris removal missions (*e.g.*, ClearSpace-1, Sunrise, Restore-L) committed to de-orbit inactive satellites in order to preserve commercial and scientific relevant orbits. In parallel to this technological effort, on-orbit servicing missions devoted to supply different services to extend the operational life of a *client satellite* (*e.g.*, inspection, repair, refueling) are being addressed, advancing the existing flight heritage from the several missions that exercised cooperative rendevous, docking, and robotic technology demonstrations (*e.g.*, Automated Transfer Vehicle,[1] ETS-VII,[2] Orbital Express,[3] PRISMA[4]). Both these categories of missions are calling for advances in several different, though interconnected, disciplines that include technical aspects (devices and algorithms) part of the relative guidance navigation and control system, the development of standards in the execution of proximity operations, mission safety policies, and legal and regulatory aspects. Both US and Europe have initiated working panels to discuss and deliver technical standards and guidelines for operational practices to enable safe commercial on-orbit operations.

This work focuses on the design of relative trajectories for CPOs, a topic which is strictly related to the definition of mission concept and operations, the safety management in the sense of inter-satellite collision avoidance, and the level of autonomy of the proximity activities. Accordingly, first a critical comparison between needs and peculiarities of the two aforementioned mission categories is carried out. Subsequently, the design is tackled in a common framework where the relative dynamics is parametrized through relative orbital elements (ROEs). In these variables, in fact, the one-orbit minimum distance in the plane perpendicular to the local transversal direction is

*Research Engineer, Department of Aerospace Science and Technology, Politecnico di Milano, 20156, Milano, Italy.
†Full Professor, Department of Aerospace Science and Technology, Politecnico di Milano, 20156, Milano, Italy.

simply expressed by the phasing of the relative eccentricity/inclination vectors. This makes ROEs a convenient choice to develop algorithms that embed collision avoidance measures based on that kind of passive safety.

CLOSE PROXIMITY OPERATIONS CONCEPTS

Figure 1 portraits different CPOs approaches applicable to on-orbit-servicing and Active Debris Removal (ADR) missions. The top-view presents the standard V-bar approach for example used by the ATV mission,[1] while the bottom-view is built on the experience collected by the AVANTI (Autonomous Vision Approach Navigation and Target Identification) in-orbit demonstration of autonomous noncooperative rendezvous.[5]

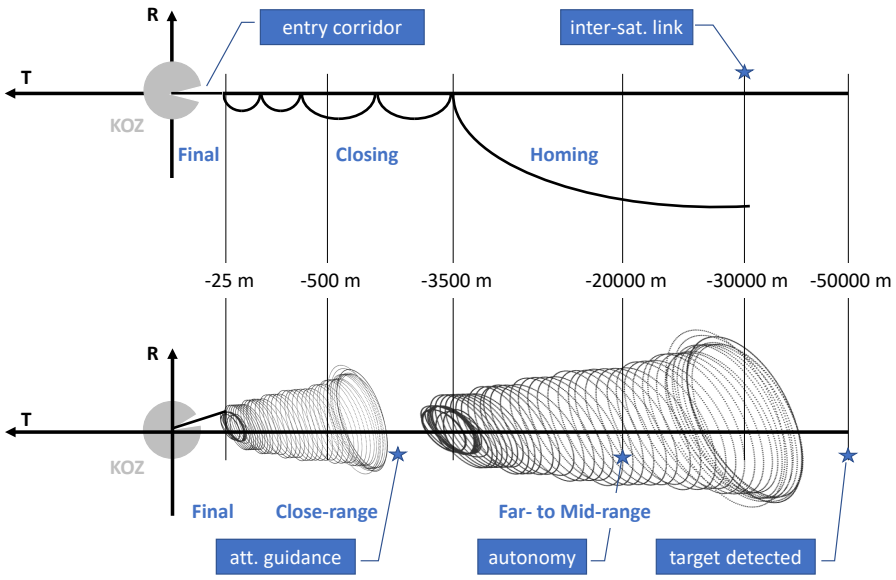

Figure 1. Possible operations concepts for CPOs (not in scale). KOZ stands for Keep Out Zone around the target.

By comparing phases and related regions of inter-satellite distance of the two approaches three main aspects deserve special consideration: the level of *cooperation* between the spacecraft, the time allocated to carry out the CPOs, and the goal of the mating phase (*i.e.*, servicing or capture). The level of cooperation is measured by the existence of some kind of communication link to exchange information between the satellites. The inter-satellite link is considered available below 30 km of separation, also based on the PRISMA experience.[4] In general cooperation guarantees the availability of a precise and reliable relative navigation solution. The time duration of the CPOs is impacted by the presence of man-it-the-loop (*i.e.*, crew), by the complexity of the relative navigation task, and by the level of autonomy required by the application. For noncooperative, autonomous, robotic missions allocating more time to perform the CPOs is important to ensure safety and to mitigate development and operations' costs. As pointed out in the lessons learned from AVANTI,[6] in fact, the transition into each next phase of the CPOs requires a sort of commissioning phase that cannot be performed without the target in sight. Note that this forces to include break points in the mission timeline to enable an adequate ground-based support at reasonable costs. Finally, the goal of the mating phase is strictly related to the level of *collaboration* between the spacecraft. A

malfunctioning or inoperative satellite is considered non-collaborative, since the target may only be capable of coarse attitude control or may even have a spinning or tumbling rotational motion.[7] Indeed, these three aspects drive the development of the mission operations concept, with direct impact on the relative trajectory design to ensure operational safety.

A convenient rendezvous strategy for noncooperative mission scenarios has been recently demonstrated by the AVANTI experiment.[8] It exploited the use of passively safe relative trajectories, where the safety is based on a proper phasing of the relative eccentricity and inclination vectors (hereafter referred as to E/I safety) and a moderate value of the relative semi-major axis.[9] In Figure 1 the target can be detected by means of a far-range camera system already at 50 km of separation, as confirmed by the AVANTI results. Autonomy is required when decreasing the separation below 20 km (depending on how important is the effect of differential aerodynamic drag perturbation) to cope with the limits of the ground segment.[5] The E/I based type of rendezvous allows decreasing both the mean inter-satellite separation in along-track direction and the size of the relative orbit, while aiding the convergence of the autonomous onboard relative navigation system.[10] Since no criticality arises from the absence of a direct measure of the inter-satellite range, simple passive camera systems can be exploited to provide angles-only observations, already achievable at large separations. Moreover, E/I safe orbits allow allocating enough time to dump the telemetry and to monitor the behavior of the onboard filter on-ground and *post-facto*.[11] As a result, this approach provides a reliable and practical solution to cover the mission phases from far- to close-range rendezvous, as well as the close-range inspection phase needed to retrieve updated information on the status of the target, to estimate its mass, inertia, and rotational motion, and to validate the behavior of the close-range pose estimation algorithms. Note that at a certain distance from the target an attitude guidance synchronized with the relative trajectory is needed to keep the target in the field of view of the sensing instruments. Afterwards, depending on the typology of capture foreseen by a mission, case-specific relative trajectories have to be designed. These in general cannot use anymore the E/I based passively safe structure and require forced motion solutions to execute prompt inbound/receding trajectories as well as fly-around trajectories with respect to any given axis of rotation, which generally is a moving direction in the local orbital frame. As such, these can be seen as the generalization of the final approach trajectories used for docking to collaborative targets.

The sequence of relative trajectories used in cooperative and collaborative mission scenarios is well established for all the different phases of the rendezvous[1] (see top-view of Figure 1). Here hold-points on the V-bar (*i.e.*, the along-track direction which is tangent to the local velocity for near-circular orbits) are usually set and straight-line segments are used only for the very final approach prior to docking to comply with a given entry corridor. Indeed, orbit determination and maneuver execution errors produce an error growing in time in the along-track direction. Nevertheless, in these cases, the overall achievable navigation accuracy is precise enough to enable to occupy safely the V-bar since the first phases of the CPOs. As discussed above, this condition is generally not valid for noncooperative scenarios, making the guidance and control strategies developed for the cooperative case not immediately applicable to missions of this kind. In that case the alternative solution is to exploit E/I passively safe trajectories, which ensure a non-vanishing separation in the plane perpendicular to the velocity[5,12] (see bottom-view of Figure 1). Unlike the V-bar hopping approach, these trajectories spiral around the along-track direction.

The design of the relative trajectories for the cooperative and collaborative cases on near-circular orbits is traditionally performed exploiting the Hill-Clohessy-Wiltshire (HCW) equations.[13] In this

work, instead, taking advantage of the Lyapunov transformation discussed in:[14]

$$\mathrm{T}(t) = \begin{bmatrix} 1 & 0 & -\cos(nt) & -\sin(nt) & 0 & 0] \\ 0 & 1 & 2\sin(nt) & -2\cos(nt) & 0 & 0 \\ 0 & 0 & 0 & 0 & \sin(nt) & -\cos(nt) \\ 0 & 0 & n\sin(nt) & -n\cos(nt) & 0 & 0 \\ -(3n)/2 & 0 & 2n\cos(nt) & 2n\sin(nt) & 0 & 0 \\ 0 & 0 & 0 & 0 & n\cos(nt) & n\sin(nt) \end{bmatrix} \tag{1}$$

where n is the mean motion of the reference near-circular orbit, those equations are rigorously transformed into the linearized equations in ROEs:

$$\begin{aligned} \Phi(t,t_0) &= \mathrm{T}^{-1}(t)\,\hat{\Phi}(t,t_0)\,\mathrm{T}(t_0) & \hat{\Phi}(t,t_0) &= \mathrm{T}(t)\,\Phi(t,t_0)\,\mathrm{T}^{-1}(t_0) \\ \mathrm{A} &= \mathrm{T}^{-1}(t)\,\hat{\mathrm{A}}\,\mathrm{T}(t) - \mathrm{T}^{-1}(t)\,\dot{\mathrm{T}}(t) & \hat{\mathrm{A}} &= \mathrm{T}(t)\,\mathrm{A}\,\mathrm{T}^{-1}(t) - \mathrm{T}(t)\,\dot{\mathrm{T}}^{-1}(t) \\ a\mathrm{B} &= \mathrm{T}^{-1}(t)\,\hat{\mathrm{B}} & \hat{\mathrm{B}} &= \mathrm{T}(t)\,a\mathrm{B} \\ \Psi &= \mathrm{T}^{-1}(t)\,\hat{\Psi} & \hat{\Psi} &= \mathrm{T}(t)\,\Psi \end{aligned} \tag{2}$$

In Eq. (2), $\hat{\bullet}$ quantities refer to the HCW dynamics, whereas the others to their respective in ROEs. Φ is the state transition matrix, A the plant matrix, B the control input matrix (the semi-major axis a of the reference orbit is used to render quantities in the unit of length), while Ψ is the convolution matrix. The ROEs used are defined as:

$$\begin{aligned} \delta\boldsymbol{\alpha} &= (\delta a, \delta\lambda, \delta e_x, \delta e_y, \delta i_x, \delta i_y)^{\mathrm{T}} \\ &= (\Delta a/a, \Delta u + \Delta\Omega\cos i, \Delta e_x, \Delta e_y, \Delta i, \Delta\Omega\sin i)^{\mathrm{T}} \end{aligned} \tag{3}$$

and are function of differences of the non-singular Keplerian elements and of the inclination i. The quantity u is the mean argument of latitude of the satellite on the reference orbit. Note that the transformation of Eq. (1) is rigorous in the absence of conservative perturbations on the relative dynamics. This is acceptable in the design of the trajectories of the final phases of the CPOs, given the limited time durations and satellite separations in play. For far- to close-range rendezvous, the ROE-based precise perturbed analytical motion is described in Reference 14. Moreover, the transformation of Eq. (1) can be seen as a mapping from the ROEs to the Cartesian relative state in the orbital co-moving RTN (Radial-Tangential-Normal) system, where tangential is used in place of transversal given the near-circular reference orbit. This is accurate when the satellite are close to each other; whereas for the design of the relative navigation filter at far-range it is advised to use its more accurate counterpart.[15]

By employing the the transformation of Eq. (1), the traditional design of CPO trajectories can be revisited in the ROEs framework. As a result, this provides a more intuitive interpretation of the safety and delta-v considerations that justified the original design. Moreover, the computation of the final approach segment can be recast as a ROE-based linear-programming problem to minimize the 1-norm of the delta-v consumption, achieving a remarkable delta-v saving for the cases that do not require a specific relative velocity profile during the approach. On the other hand, as discussed above, relative trajectories for noncooperative rendezvous are conveniently designed directly in the ROE space. Hence, the capability to perform the trajectory design in a common framework for all the applications makes the comparison extremely effective and supports possible cross synergies between different strategies. Finally, the trajectory design for the capture phase in non-collaborative

scenarios can benefit from merging known elementary solutions developed in the Cartesian frame (*e.g.*, 3D straight-line segments and fly-around orbits) to the geometric insight provided in terms of ROEs.

COOPERATIVE-COLLABORATIVE CASE IN ROES

In this section, known analytical impulsive maneuver schemes are revisited in terms of ROEs.

Insight in the impulsive 2-burn solution

In the linearized unperturbed relative dynamics the in-plane and out-of-plane motions are decoupled. To achieve an out-of-plane only reconfiguration by means of two impulsive burns, the solution based on the HCW equations is singular when the burns are spaced by $\pi + k\pi$ in mean argument of latitude.[1] Under the ROE perspective it can be noted that such singularity can be avoided by including the additional constraint on the u^* of the burns:

$$\mathrm{mod}\ (u^*, \pi) = \quad \mathrm{mod}\ \left(\arctan\left(\frac{\Delta\delta i_y}{\Delta\delta i_x} \right), \pi \right) \tag{4}$$

which relates the maneuver location to the total change of the relative inclination vector during the reconfiguration. Then at such mean argument of latitude, the solution $u_1 = u^*$, $u_2 = u_1 + k\pi$ exists and it is delta-v optimal.[16] The geometrical interpretation of delta-v optimality in the relative inclination plane discussed in Reference 16 suggests that when u^* is not contained in the reconfiguration horizon $[u_0, u_\mathrm{F}]$ (*i.e.*, the reconfiguration is performed in less than half orbital period not containing the optimal value of the mean argument of latitude), the cheapest solution is to maneuver at the initial and final times. The numerical evidence of that is provided in Figure 2, where the example of a reconfiguration that changes the y-component only of the relative inclination vector of 250 m is considered. In this case $\mathrm{mod}\ (u^*, \pi) = \pi/2$, marked by dashed vertical lines. The minimization of the $\|\delta\mathbf{v}\|_1$ cost is found when the maneuvers are performed at the extrema of the intervals (right-view), though achieving a cost sub-optimal w.r.t. maneuvering at u^*. Moreover, the shorter the reconfiguration time, the larger the delta-v required (left-view).

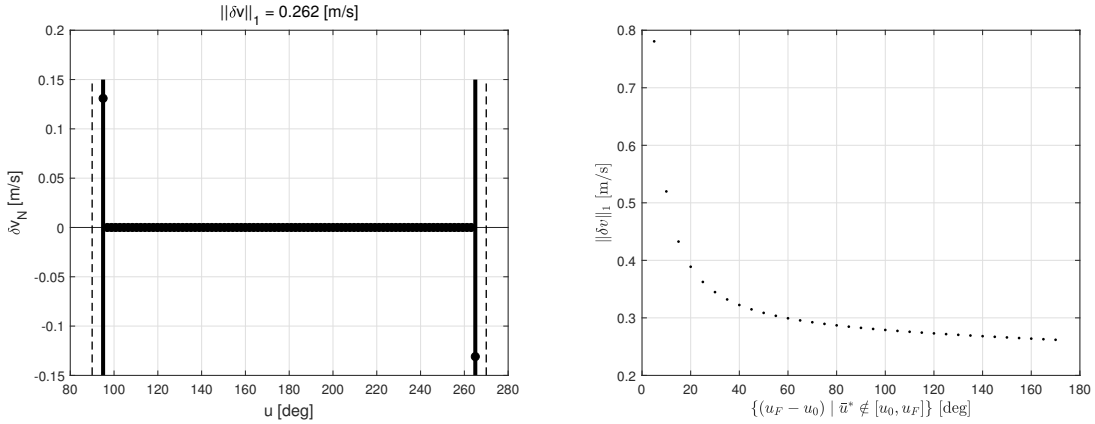

a) Delta-v minimum solution when $u^* \notin [u_0, u_\mathrm{F}]$. b) Delta-v cost at varying $[u_0, u_\mathrm{F}]$.

Figure 2. Two-impulses out-of-plane reconfiguration.

As for the in-plane (ip) reconfiguration, the HCW solution is singular when the burns are spaced by $2\pi + 2k\pi$. The ROE solution can be written as:

$$\begin{bmatrix} 0 & 2 & 0 & 2 \\ -2 & -3(u_{\mathrm{F}} - u_0) & -2 & 0 \\ \sin u_0 & 2\cos u_0 & \sin u_{\mathrm{F}} & 2\cos \mathrm{F} \\ -\cos u_0 & 2\sin u_0 & -\cos u_{\mathrm{F}} & 2\sin u_{\mathrm{F}} \end{bmatrix} \begin{pmatrix} \delta v_{\mathrm{R}0} \\ \delta v_{\mathrm{T}0} \\ \delta v_{\mathrm{RF}} \\ \delta v_{\mathrm{TF}} \end{pmatrix} = an\Delta\delta\boldsymbol{\alpha}_{ip} \tag{5}$$

One could try to remove the singularity as done for the out-of-plane case (*i.e.*, by adding a constraint on the u and excluding the radial component of the second burn to obtain three equations that can be inverted). Nevertheless, in this case the ratio between the 3rd and 4th equations of Eq. (5) cannot be solved for a u^* that depends only on the total change of the relative eccentricity vector. This method is actually what it is employed for the 3-impulse-tangential optimal solution.[16] But the presence of radial components in the delta-v do not allow this solution in this case. As a result, the singularity cannot be avoided. In practice one can simply take an interval shorter/longer than 2π, or can consider to perform more burns. An overview of the possible solutions for the 2 or 3 burns cases is provided in Tables 1 and 2 of Reference 16.

The traditional burn schemes adopted for closing hops between hold-points on the V-bar

Two-burns analytical schemes are often exploited to perform closing hops on the the V-bar between two hold-points (*i.e.*, only $a\delta\lambda \neq 0$ in ROEs). Three possibilities can occur, namely: couple of T only maneuvers, couple of R only maneuvers, and the general solution RT-RT.

As for the T-T 2-burn scheme, from the expressions in ROEs of Eq. (5) one derives that: $\delta v_{\mathrm{T}0} = -\delta v_{\mathrm{TF}}$, $a\Delta\delta\lambda$ is fixed equal to $-(3/n)(u_{\mathrm{F}} - u_0)\delta v_{\mathrm{T}0}$ and this determines also the sign of $\delta v_{\mathrm{T}0}$. To satisfy the boundary conditions on the relative eccentricity vector, the $\xi = (u_{\mathrm{F}} - u_0) = 2\pi$. This is the delta-v cheapest solution, but it establishes a drift towards target that is operationally dangerous in the case of missed second burn. For this reason this solution is not used in practice.

As for the R-R 2-burn scheme, from the expressions in ROEs of Eq. (5) one derives that: $a\Delta\delta\lambda$ is fixed equal to $-(2/n)(\delta v_{\mathrm{R}0} + \delta v_{\mathrm{RF}})$. In order to satisfy the boundary conditions on the relative eccentricity vector the two additional conditions of $u_{\mathrm{F}} = u_0 + k\pi$ and $\delta v_{\mathrm{R}0} = \delta v_{\mathrm{RF}}$ are needed. This solution is more expensive than the previous one but, in case of missed second burn, the relative motion is bounded (*i.e.*, nominally no residual drift is present). This aspect made this solution employed in missions as ATV.

The last case foresees the use of a RT-RT 2-burn scheme. From the expressions in ROEs of Eq. (5) and by considering a $\xi < 2\pi$ (thus excluding the value $\xi = 2k\pi$) one derives that $\delta v_{\mathrm{T}0} = -\delta v_{TF}$ and $\delta v_{\mathrm{R}0} = \delta v_{\mathrm{R}F}$, in agreement with both the special cases discussed above. Moreover, having fixed start and end points on the V-bar the radial component of the Cartesian relative state is $x_0 = x_{\mathrm{F}} = 0$. By choosing $\xi < \pi$ it derives that the tangential component of the velocity before the second burn is $v_T^-(t_{\mathrm{F}}) > 0$ (for an approach from the -V-bar). This latter is a *structural* passive abort safety condition, since in case of missed second burn, the trajectory will not get closer to the target than $y(t_{\mathrm{F}})$ and the residual drift makes the approaching satellite moving back away from the target. Note that this absence of overshoot occurs when start and end conditions are hold-points on the V-bar.

Overview of proposed guidance profiles for the V-bar approach

Based on the simple 2-burn solutions discussed before, several guidance profiles have been implemented to cover a V-bar approach with multiple burns between the initial and final hold-point

states. In this section an overview is provided, with special attention to the Passive Abort (PA) safety behavior. This latter is related to the relative trajectory that the approaching satellite has in case of interrupted guidance profile: a PA safe solution is a trajectory that will not lead to any collision for a given interval of time following the first missed burn. PA safety is relevant for the design to cope with major system failures that prevent the use of the propulsion system at a certain time during the approach.

For missions of the space shuttle program and within the ATV program a given relative velocity profile was also set to cover the aimed displacement while satisfying additional requests *e.g.* to decelerate when getting closer to the target or to have a given residual relative velocity at the final point.[1,17] An example is provided by the glide-slope straight path algorithm of Hablani et al.,[17] which defines a distance to go ρ quantity and sets a linear relationship between ρ and its time derivative $\dot{\rho}$. As a results, once that the number of burns N is set (equally-spaced in time and hence in u) the trajectory intersects the straight path line so that hops size decreases while getting towards the target. Having imposed a relative velocity profile (*i.e.*, the relation between ρ and $\dot{\rho}$) there are no remaining degrees of freedom and the values of the delta-vs are computed as sequences of couples of RT-RT maneuvers. As for an example, the results for a reconfiguration from -1000 m to -100 m on the V-bar is depicted in Figure 3.a. Here $N = 10$ and the relative velocity profile is tuned to obtain a total reconfiguration time of circa one orbital period (at the considered height of 775 km). In the plot, the nominal rendezvous profile is marked in solid-bold, while dashed lines represent the trajectories after each $N + 1$ missed burn.

The glide-slope algorithm is valid for whatever fixed 3D straight path in the RTN, nonetheless for the V-bar case the same result can be achieved by exploiting sequences of RT-RT burns as discussed in the previous sub-section. In this case, in fact, it is enough to ensure that the constant Δu between the burns is less than π and that the distribution of the way-points on the V-bar is chosen so that the larger steps in $a\Delta\delta\lambda$ are performed at the beginning and the smaller near the end-condition. This helps in reducing the size of the hops of the relative trajectory in terms of maximum displacement from the V-bar (*e.g.*, to minimize line-of-sight changes or to respect entry corridor conditions). In Figure 3.b the hops size is designed to be proportional to the distance to target. With $N = 10$ and total reconfiguration time of one orbital period, the same profile of before is obtained. Note that differently to the 2-burn solution between start and end hold-points, here a bit of overshoot in along-track is present for the PA segments of trajectory due to a slightly different component in the tangential delta-vs.

For the V-bar case, R only hops could also be performed in sequence. In this case one has to either relax the condition on the total time or the one on the number of burns, given the structural constraint of $\Delta u = k\pi$ to obtain radial only maneuvers. For the sake of the comparison, in Figure 4.a, the first option is pursued. As expected, the PA segments of trajectory are bounded relative orbits. Moreover, this solution (valid only for the V-bar case) is cheaper in terms of delta-v consumption. Note that since the total delta-v cost is proportional to the overall change in mean argument of longitude $a\Delta\delta\lambda$, the cost of the $N = 2$ solution is the same. The differences are on the size of the hops and the total time to cover the rendezvous.

Several works in the literature propose to write the final approach as a multiple-burn optimization problem where the overall delta-v consumption is minimized.[18,19] In the near-circular case, this problem can be recast as a Linear-Programming (LP) optimization where the delta-v cost is expressed by the norm-1 of the delta-vs, to properly model the fuel consumption in the case of 3D maneuverability. Accordingly, the following constraints are set: start- and end-conditions, total

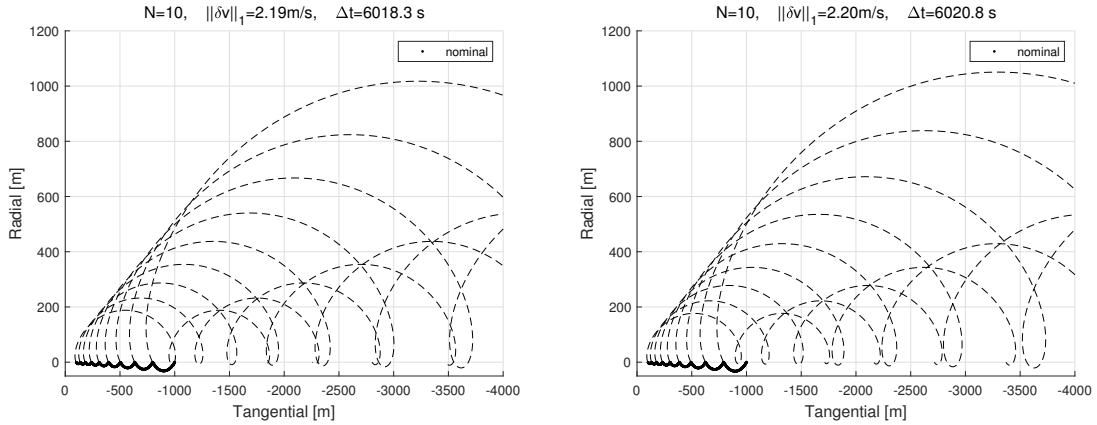

a) Glide-slope profile of 17. b) Guidance profile by means of RT-RT.

Figure 3. Comparison of V-bar approaches: nominal and N-missed burn cases.

time for the rendezvous, and number of impulsive burns to be executed. The latter are generally taken equally distributed in time. This problem can be written as a minimization problem since no specific relative velocity profile is imposed. As for the V-bar approach, additional way-point constraints can be enforced as done in Reference 19 to limit the trajectory displacement from the V-bar, as an alternative method to reduce the line-of-sight excursion. In Figure 4.b the same reconfiguration considered so far is performed using the solution of a LP problem written in ROEs. Here $N = 10$ (equally spaced in time) and $N - 2$ way-points on the V-bar are prescribed. As a result, the hops are equal in size since only the first and last maneuvers have a non-null tangential component; whereas all the intermediate burns are R only maneuvers. Indeed, the delta-v cost is less than what achieved for the profiles of Figure 3. However, the residual drift of the PA trajectory segments is larger and equal at all the times, as the drift is only canceled by the last burn performed at the arrival point.

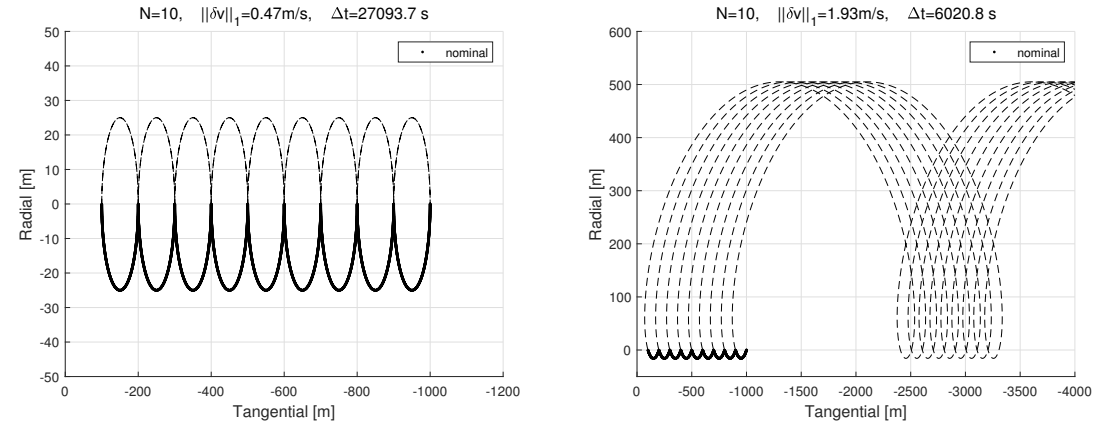

a) R-only hops (N=10). b) ROE-based LP problem with way-points.

Figure 4. Comparison of V-bar approaches: nominal and N-missed burn cases.

Table 1 collects the comparison of the profiles discussed so far in terms of spacing of the burns, corresponding way-points on the V-bar, and trajectory overshoot in case of missed burn. This latter

Table 1. Comparison of the different V-bar approaches.

N	1	2	3	4	5	6	7	8	9	10
Figure 3.a:	Δt [s]	668.7	668.7	668.7	668.7	668.7	668.7	668.7	668.7	668.7
overshoot	% [-]	7.6	7.7	7.9	8.1	8.4	8.8	9.3	10.1	11.2
y [m]	-1000.0	-798.6	-635.6	-503.6	-396.6	-310.1	-240.0	-183.2	-137.2	-100.0
Figure 3.b:	Δt [s]	669.0	669.0	669.0	669.0	669.0	669.0	669.0	669.0	669.0
overshoot	% [-]	7.9	8.0	8.1	8.2	8.4	8.7	9.2	9.8	10.5
y [m]	-1000.0	-792.0	-626.0	-493.0	-387.0	-302.0	-234.0	-179.0	-135.0	-100.0
Figure 4.a:	Δt [s]	3010.4	3010.4	3010.4	3010.4	3010.4	3010.4	3010.4	3010.4	3010.4
overshoot	% [-]	0.0	0.0	0.0	0.0	0.0	0.0	0.0	0.0	0.0
y [m]	-1000.0	-900.0	-800.0	-700.0	-600.0	-500.0	-400.0	-300.0	-200.0	-100.0
Figure 4.b:	Δt [s]	669.0	669.0	669.0	669.0	669.0	669.0	669.0	669.0	669.0
overshoot	% [-]	3.3	3.7	4.3	5.0	6.0	7.5	10.0	15.0	30.0
y [m]	-1000.0	-900.0	-800.0	-700.0	-600.0	-500.0	-400.0	-300.0	-200.0	-100.0

quantity is measured as the percentage of the distance (towards the target) in along-track direction with respect to the nominal position on the V-bar.

THE ROE-BASED LP PROBLEM

Designing the final phase of the CPOs as a LP problem is attractive considering the availability of robust solvers and the possibility to generalize the design for 3D - also time-varying for non-collaborative cases - approaches, while including different constraints that convey the requirements during that close-range approach. In this framework, exploiting the description in ROEs allows benefiting from the straightforward physical interpretation discussed so far, moreover achieving a very compact formulation of the problem matrices.

In its simplest formulation the problem is structured as:

$$\begin{array}{ll} \min & \mathrm{C}^{\mathrm{T}}\mathbf{X} \\ \text{s.t.} & A_{in}\mathbf{X} \leq \mathbf{b}_{in} \\ & A_{eq}\mathbf{X} = \mathbf{b}_{eq} \end{array} \tag{6}$$

where $\mathbf{X}$ is the vector of state variables containing the N impulsive delta-vs in RTN and the N slack variables $\mathbf{d}$ required to handle the minimization of the 1-norm in a LP fashion:

$$\begin{array}{rcl} \mathbf{X}^{\mathrm{T}} & = & \left(\begin{array}{cccccc} \delta\mathbf{v}_0^{\mathrm{T}} & \cdots & \delta\mathbf{v}_{N-1}^{\mathrm{T}} & \mathbf{d}_0^{\mathrm{T}} & \cdots & \mathbf{d}_{N-1}^{\mathrm{T}} \end{array} \right) \\ \mathrm{C}^{\mathrm{T}} & = & \left(\begin{array}{cccc} \mathrm{O}_{1\times 3N} & 1 & \cdots & 1 \end{array} \right) \end{array} \tag{7}$$

The inequality constraints convey the minimization of the norm-1 through the slack variables $\mathbf{d}_0^{\mathrm{T}}$ $\cdots$ $\mathbf{d}_{N-1}^{\mathrm{T}}$ as follows:

$$A_{in} = \left[\begin{array}{cc} \mathrm{I}_N \otimes \mathrm{I}_3 & -\mathrm{I}_N \otimes \mathrm{I}_3 \\ -\mathrm{I}_N \otimes \mathrm{I}_3 & -\mathrm{I}_N \otimes \mathrm{I}_3 \end{array} \right] \qquad \mathbf{b}_{in} = \left(\begin{array}{c} \mathrm{O}_{3N\times 1} \\ \mathrm{O}_{3N\times 1} \end{array} \right) \tag{8}$$

where I_N denotes the $N \times N$ identity matrix, $\mathrm{O}_{i\times j}$ the null matrix of dimension $i \times j$, and $\otimes$ is the Kronecker product. The equality constraints are used to enforce the end-conditions at the end-time and are given by:

$$A_{eq} = \left[\begin{array}{ccc} \Phi_{\mathrm{F},0}\, a\mathrm{B}_0 & \cdots & a\mathrm{B}_{\mathrm{F}} \end{array} \right] \qquad \mathbf{b}_{eq} = a\delta\boldsymbol{\alpha}_{\mathrm{F}} - \Phi_{\mathrm{F},0}\, a\delta\boldsymbol{\alpha}_0 \tag{9}$$

where the short-hand notation $\Phi_{i,j}$ is used to express $\Phi(u_i, u_j)$ and $a\mathrm{B}_i$ for $a\mathrm{B}(u_i)$.

The formulation of Eq. (6) can be used to verify the known ROE-based theoretical results presented in Reference 16. When shorter reconfiguration time horizons are considered instead, Eq. (6) can identify more convenient solutions that make use of combined in-plane and out-of-plane maneuvers. As for the example used so far, as expected, the solution would be to burn at initial and end times with T only maneuvers, scoring a delta-v cost of 0.1 m/s. Nevertheless, as discussed in previous sections, this solution is not operationally practicable since in case of missed second burn the residual drift is towards the target. Finally, by exploiting the facts that ROE variables introduce negligible linearization errors and an accurate first order state transition matrix for the perturbed motion is available, this approach can be used also for the far- to close-range rendezvous. In this case, to further reduce the size of the matrices, the times of the N burns could be provided in agreement with the optimal u candidates known from the analysis of the reconfiguration in the ROE space. As such, this methodology would be an alternative to the approach used in AVANTI, where the minimization of the square of the norm-2 of the delta-v was pursued instead (single direction thruster).

The results of Figure 4.b were obtained by imposing $N-2$ way-points on the straight path line of the rendezvous (in that case the V-bar direction). This requires to extend the state variable by $N-2$ ζ scalar variables, used to parametrize the approach segment:

$$\tilde{\mathbf{X}}^{\mathrm{T}} = \begin{pmatrix} \zeta_1 & \cdots & \zeta_{N-2} & \mathbf{X}^{\mathrm{T}} \end{pmatrix} \tag{10}$$

and the related equality constraints are given by:

$$A_{eq\mathrm{WP}} = \begin{bmatrix} \mathrm{I}_{N-2} \otimes \mathrm{M} & \tilde{\mathrm{A}} & \mathrm{O}_{3(N-2)\times N} \end{bmatrix} \qquad \mathbf{b}_{eq\mathrm{WP}} = \begin{pmatrix} \tilde{\mathrm{T}}_1 \Phi_{1,0} a\delta\boldsymbol{\alpha}_0 - \mathbf{x}_0 \\ \vdots \\ \tilde{\mathrm{T}}_{N-2} \Phi_{N-2,0} a\delta\boldsymbol{\alpha}_0 - \mathbf{x}_0 \end{pmatrix} \tag{11}$$

where $\mathrm{M} = \mathbf{x}_{\mathrm{F}} - \mathbf{x}_0$ defines the approach segment in RTN and $\tilde{\mathrm{T}}_i$ is the 3×6 position sub-block of the transformation T_i of Eq. (1) evaluated at time u_i. The remaining quantity $\tilde{\mathrm{A}}$ is:

$$\tilde{\mathrm{A}} = \begin{bmatrix} -\tilde{\mathrm{T}}_1 \Phi_{1,0}\, a\mathrm{B}_0 & \mathrm{O}_{3\times 3} & \cdots & \mathrm{O}_{3\times 3} \\ \vdots & \ddots & & \vdots \\ -\tilde{\mathrm{T}}_{N-2} \Phi_{N-2,0}\, a\mathrm{B}_0 & -\tilde{\mathrm{T}}_{N-2} \Phi_{N-2,N-3}\, a\mathrm{B}_{N-3} & \mathrm{O}_{3\times 3} & \mathrm{O}_{3\times 3} \end{bmatrix} \tag{12}$$

For the final approach to target entry corridor or Line-OF-Sight (LOS) constraints are generally required to avoid collision with appendages or to respect the field of view characteristics of the close-range relative navigation sensors. These can be expressed by the polytope:

$$A_{\mathrm{L}} = \begin{bmatrix} -1 & 0 & 0 \\ -1 & +\rho & 0 \\ -1 & -\rho & 0 \\ -1 & 0 & +\rho \\ -1 & 0 & -\rho \end{bmatrix} \qquad \mathbf{b}_{\mathrm{L}} = \begin{pmatrix} -x_{\mathrm{lim}} \\ \mathrm{O}_{5\times 1} \end{pmatrix} \tag{13}$$

where $\rho = \tan(\pi/2 - \alpha)$, with α the aperture angle of the semi-cone w.r.t. the boresight, and x_{lim} is the distance along the boresight from the center of mass to the satellite side. These quantities are

defined in the sensor/corridor reference system centered on the target center of mass (denoted by the superscript s), where the boresight is aligned to the $+x$ direction. Accordingly, the constraints are given by: $A_{\mathrm{L}}\mathbf{x}_i^{\mathrm{s}} \leq \mathbf{b}_{\mathrm{L}}$ at a given time i. For the LP formulation the matrix of LOS inequality constraints are then assembled as:

$$A_{in\mathrm{LOS}} = \begin{bmatrix} A_{\mathrm{L}}\mathrm{R}_1\tilde{\mathrm{T}}_1\Phi_{1,0}\,a\mathrm{B}_0 & \mathrm{O}_{3\times3} & \cdots & \mathrm{O}_{3\times3} \\ \vdots & \ddots & & \vdots \\ A_{\mathrm{L}}\mathrm{R}_{N-2}\tilde{\mathrm{T}}_{N-2}\Phi_{N-2,0}\,a\mathrm{B}_0 & \cdots & A_{\mathrm{L}}\mathrm{R}_{N-2}\tilde{\mathrm{T}}_{N-2}\Phi_{N-2,N-2}\,a\mathrm{B}_{N-2} & \mathrm{O}_{3\times3} \end{bmatrix}$$

$$\mathbf{b}_{in\mathrm{LOS}} = \begin{pmatrix} \mathbf{b}_{\mathrm{L}} - A_{\mathrm{L}}\mathrm{R}_1\tilde{\mathrm{T}}_1\Phi_{1,0}\,a\delta\boldsymbol{\alpha}_0 \\ \vdots \\ \mathbf{b}_{\mathrm{L}} - A_{\mathrm{L}}\mathrm{R}_{N-2}\tilde{\mathrm{T}}_{N-2}\Phi_{N-2,0}\,a\delta\boldsymbol{\alpha}_0 \end{pmatrix} \tag{14}$$

where R_i is the rotation matrix from the s to the RTN frame evaluated at time u_i. The results of including the LOS constraints in the V-bar approach considered so far are presented in Figure 5, with α of 15 degrees. The fact that the constraints are imposed only at the given N times is responsible for the slight violation of the LOS border by the propagated trajectory. This can be mitigated either defining the cone amplitude with some margin or using convex optimization schemes to enforce the validity of the constraints continuously in the convex closed polytope of Eq. (13).

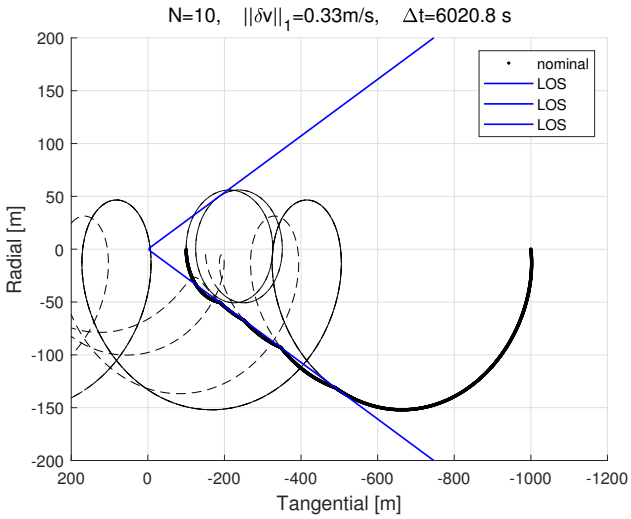

Figure 5. V-bar approach with LOS constraints.

Within the LP formulation also a certain form of PA safety can be included as additional constraint. In this case the following open polytope can be used to define the region in the reference system with $+x$ directed and opposite to the direction of the approach:

$$A_{\mathrm{PA}} = \begin{bmatrix} -1 & 0 & 0 \end{bmatrix} \qquad b_{\mathrm{PA}} = -x_{\mathrm{limDS}} \tag{15}$$

where x_{limDS} is the distance along the approach direction from the center of mass of the target to the panel on the docking side. The quantities in Eq. (15) are expressed in a target-centered reference system (denoted by the superscript bf), to convey: $A_{\mathrm{PA}}\mathbf{x}_i^{\mathrm{bf}} \leq \mathbf{b}_{\mathrm{PA}}$ at a given time i. The objective is to check that the trajectory after a given missed burn, propagated for a certain time, will not enter the

region described by the polytope. The LP formulation can handle this only if the region is convex. The following service matrices are introduced:

$$\mathrm{Z}_{i,j} = \begin{bmatrix} A_{\mathrm{PA}}\mathrm{R}_i\tilde{\mathrm{T}}_i\Phi_{i,j}\, a\mathrm{B}_j \\ \vdots \\ A_{\mathrm{PA}}\mathrm{R}_M\tilde{\mathrm{T}}_M\Phi_{M,j}\, a\mathrm{B}_j \end{bmatrix} \qquad \mathrm{K}_i = \begin{bmatrix} A_{\mathrm{PA}}\mathrm{R}_i\tilde{\mathrm{T}}_i\Phi_{i,0}\, a\delta\boldsymbol{\alpha}_0 \\ \vdots \\ A_{\mathrm{PA}}\mathrm{R}_M\tilde{\mathrm{T}}_M\Phi_{M,0}\, a\delta\boldsymbol{\alpha}_0 \end{bmatrix} \tag{16}$$

to respectively provide the propagated trajectory at all times from i to M starting from the last performed burn $\delta\mathbf{v}_j$ or the initial condition $a\delta\boldsymbol{\alpha}_0$. The number of points M and the duration of time to check the propagated trajectory after each last performed burn are set as input to the solver. M turns into additional constraints on the $\mathbf{X}$ variables (*i.e.*, additional rows of each $\mathrm{Z}_{i,j}$ block). In Eq. (16) R_i denotes the rotation matrix from the bf to the RTN frame evaluated at time u_i. Accordingly, the matrices of convex PA safety equality constraints are then assembled as:

$$A_{eq\mathrm{PA}} = \begin{bmatrix} \mathrm{Z}_{1,0} & \mathrm{O}_{N-1+M\times 3} & \cdots & \mathrm{O}_{N-1+M\times 3} \\ \mathrm{Z}_{2,0} & \mathrm{Z}_{2,1} & \cdots & \mathrm{O}_{N-2+M\times 3} \\ \vdots & \ddots & & \vdots \\ \mathrm{Z}_{N,0} & \mathrm{Z}_{N,1} & \cdots & \mathrm{Z}_{N,N} \end{bmatrix}$$
$$\mathbf{b}_{eq\mathrm{PA}} = \begin{pmatrix} b_{\mathrm{PA}} - \mathrm{K}_1 \\ \vdots \\ b_{\mathrm{PA}} - \mathrm{K}_N \end{pmatrix} \tag{17}$$

The results of including the convex PA safety constraints in the V-bar approach considered so far are presented in Figure 6, where x_{limDS} is set to 90 m and the safety is checked for 7 orbits after each burn (to emulate an interruption of the guidance profile).

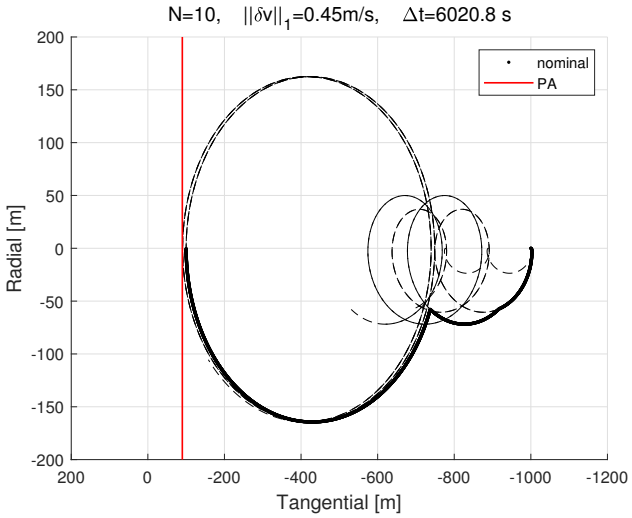

Figure 6. V-bar approach with convex PA safety constraints.

The simultaneous enforcement of different types of constraints is critical, since it is not ensured that a feasible solution exists. In Figure 7 are shown the examples where first PA safety and LOS constraints are set (right-view), then way-points and LOS are set (left-view). In the first case a

solution satisfying PA safety can be found. In the second case, enforcing way-points (*i.e.*, position at a certain time) leaves no degrees of freedom to the maneuvers to satisfy also the PA safety needs. In this case, LOS constraints become inactive.

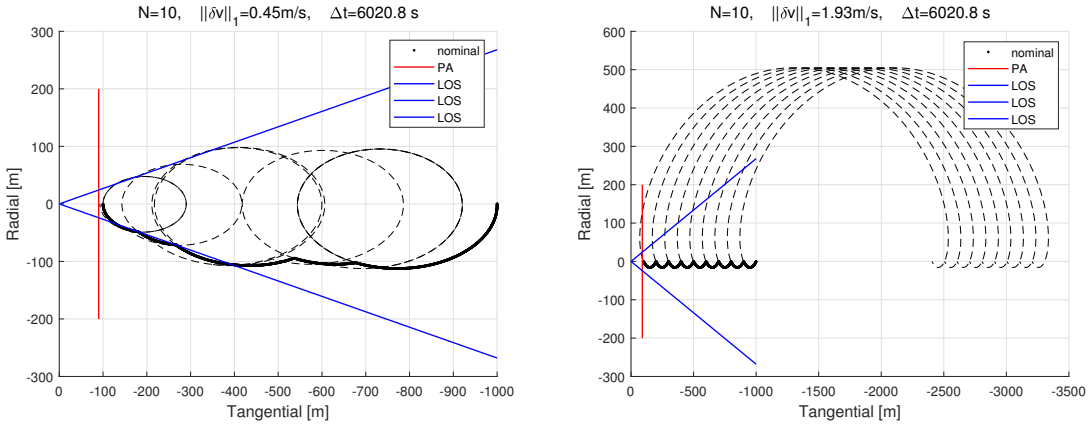

a) PA safety and LOS constraints.

b) Way-points and LOS constraints.

Figure 7. V-bar approaches subject to multiple constraints.

Indeed the V-bar approach is a particular case, both for the nature of the relative dynamics and for the deep understanding of the solution that one can derive. The solution of the general 3D case, and especially in the case where the constraints are time dependent due to the rotation of the target as seen in the RTN frame, is more demanding indeed. As an example Figure 8 presents the in-plane view of a 3D approach to docking or capture. In this case initial and final positions in RTN are respectively: $(35.4, -35.4, 20)^{\mathrm{T}}$ and $(1.4, -1.4, 0)^{\mathrm{T}}$ meters. There, only the PA safety constraints are set, with limit of 1.4 meters and checked for one orbital period after each performed burn. In order to find a solution, the reconfiguration time is assumed as one orbital period, which may be definitely long for a prompt action in ADR scenarios. The obtained solution is clearly very far away from the straight line solution. For the same 3D final approach the cases in which path constraints are included are presented in Figure 9. In these cases both solutions are possible, moreover with comparable costs and compatibly with shorter reconfiguration time (in this case it is set equal to 20 minutes). As it can be seen, the convex PA safety cannot be respected, especially for the last maneuvers in proximity of the end conditions. This suggests either the need to formulate PA safety in proximity of the contact in a less stringent fashion than the adopted convex one or to include an active safety policy for the very last phases. The latter, however, requires that the failure is not so critical to prevent firing and could cause some impingement perturbation on the target due to the escape maneuver.

CONCLUSION

This work investigated the design of relative trajectories required by the operational concepts of a large class of on-orbit servicing missions. Focus has been given on safety aspects, mainly in the sense of passive abort safety. To enhance the understanding of the problem set-up and of the obtained solutions, the relative orbital elements framework has been exploited. Given the simplicity of the adopted solver, the proposed methodologies can be used to support the development of guidance and control algorithms for spaceborne implementations.

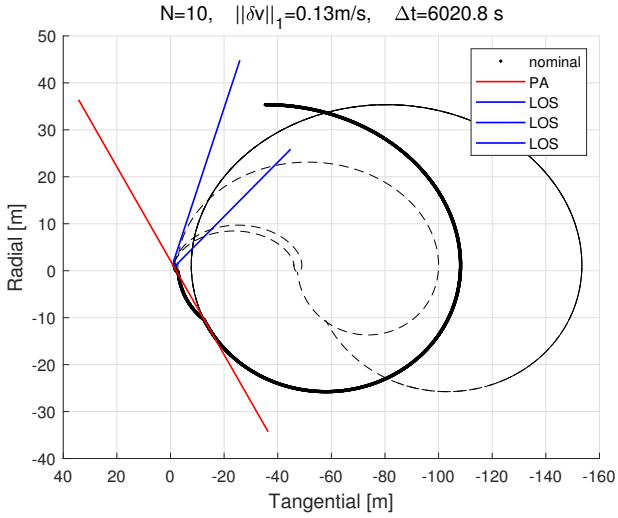

Figure 8. 3D final approach subject to convex PA safety constraints.

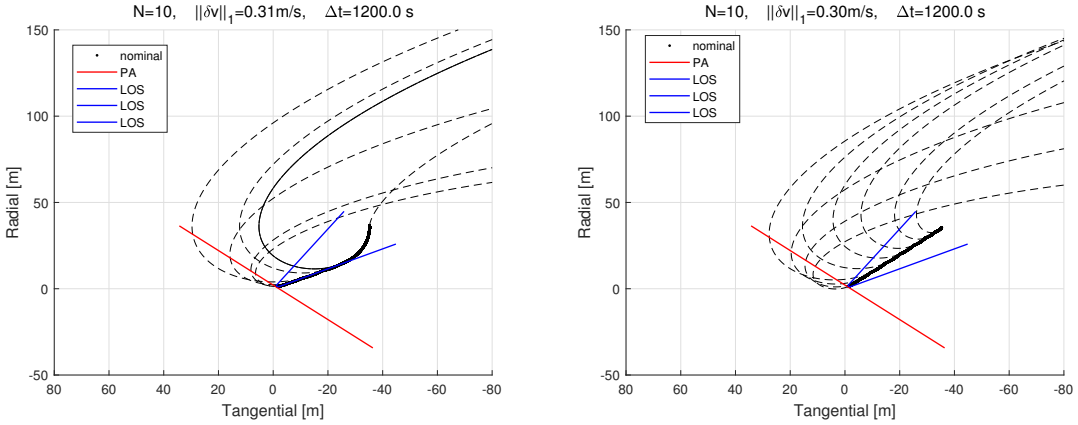

a) Only LOS constraints. b) Only Way-points constraints.

Figure 9. 3D final approach subject to path constraints.

ACKNOWLEDGMENT

The research leading to these results has received funding from the European Union's Horizon 2020 research and innovation programme under the Marie Skłodowska-Curie grant agreement No 793361 – ReMoVE (Rendezvous Modelling Visiting and Enhancing).

REFERENCES

[1] F. Ankersen, *Guidance, Navigation, Control and Relative Dynamics for Spacecraft Proximity Maneuvers*. PhD thesis, Aalborg University, Denmark, Dec. 2010.

[2] M. Oda, "Summary of NASDA's ETS-VII robot satellite mission," *Journal of Robotics and Mechatronics*, Vol. 12, No. 4, 2000, pp. 417–424, 10.20965/jrm.2000.p0417.

[3] T. Weismuller and M. Leinz, "GN&C Technology Demonstrated by the Orbital Express Autonomous Rendezvous and Capture Sensor System," No. Paper 06-016, 29th Annual AAS Guidance and Control Conference, American Astronautical Society, 2006.

[4] P. Bodin, R. Noteborn, R. Larsson, T. Karlsson, S. D'Amico, J.-S. Ardaens, M. Delpech, and J.-C. Berges, "PRISMA Formation Flying Demonstrator: Overview and Conclusions from the Nominal Mission," No. 12-072, Breckenridge, Colorado, USA, 35th Annual AAS Guidance and Control Conference, 2012.

[5] G. Gaias and J.-S. Ardaens, "Flight Demonstration of Autonomous Noncooperative Rendezvous in Low Earth Orbit," *Journal of Guidance, Control, and Dynamics*, Vol. 41, No. 6, 2018, pp. 1137–1354. https://doi.org/10.2514/1.G003239.

[6] G. Gaias and J.-S. Ardaens, "In-orbit experience and lessons learned from the AVANTI experiment," *Acta Astronautica*, Vol. 153, 2018, pp. 383–393. 10.1016/j.actaastro.2018.01.042.

[7] G. Borelli, G. Gaias, and C. Colombo, "Rotational control with plume impingement to aid the rigid capture of an uncooperative failed satellite," No. AAS-20-670, Lake Tahoe, CA, USA, AAS/AIAA Astrodynamics Specialist Conference, 2020.

[8] G. Gaias, C. Colombo, and M. Lara, "Analytical Framework for Precise Relative Motion in Low Earth Orbits," *Journal of Guidance, Control, and Dynamics*, Vol. 43, No. 5, 2020, pp. 915–927. Article in Advance (published online 14 Mar 2020), doi: 10.2514/1.G004716.

[9] G. Gaias and J.-S. Ardaens, "Design challenges and safety concept for the AVANTI experiment," *Acta Astronautica*, Vol. 123, 2016, pp. 409–419. doi: 10.1016/j.actaastro.2015.12.034.

[10] J.-S. Ardaens and G. Gaias, "Flight Demonstration of Spaceborne Real-Time Angles-Only Navigation to a Noncooperative Target in Low-Earth Orbit," *Acta Astronautica*, Vol. 153, 2018, pp. 367–382. 10.1016/j.actaastro.2018.01.044.

[11] J.-S. Ardaens and G. Gaias, "Angles-Only Relative Orbit Determination in Low Earth Orbit," *Advances in Space Research*, Vol. 31, No. 11, 2018, pp. 2740–2760. 10.1016/j.asr.2018.03.016.

[12] M. A. Vavrina, C. E. Skelton, K. D. DeWeese, B. J. Naasz, D. E. Gaylor, and C. D'Souza, "Safe Rendezvous Trajectory Design for the Restore-L Mission," No. AAS-19-410, Ka'anapali, HI, 29th AAS/AIAA Space Flight Mechanics Meeting, 2019.

[13] W. H. Clohessy and R. S. Wiltshire, "Terminal Guidance System for Satellite Rendezvous," *Journal of the Aerospace Sciences*, Vol. 27, No. 9, 1960, pp. 653–658.

[14] G. Gaias and M. Lovera, "Trajectory design for proximity operations: the relative orbital elements' perspective," *Journal of Guidance, Control, and Dynamics*. under peer review process.

[15] G. Gaias, J.-S. Ardaens, and C. Colombo, "Precise Line-of-Sight Modelling for Angles-Only Relative Navigation.," *Advances in Space Research*, 2020. in press. doi: 10.1016/j.asr.2020.05.048.

[16] G. Gaias and S. D'Amico, "Impulsive Maneuvers for Formation Reconfiguration using Relative Orbital Elements," *Journal of Guidance, Control, and Dynamics*, Vol. 38, No. 6, 2015, pp. 1036–1049. doi: 10.2514/1.G000191.

[17] H. Hablani, M. Tapper, J. David, and D. DanaBashian, "Guidance and relative navigation for autonomous rendezvous in a circular orbit," *Journal of Guidance, Control and Dynamics*, Vol. 25, No. 3, 2002, pp. 553–562.

[18] L. Breger and J. P. How, "Safe Trajectories for Autonomous Rendezvous of Spacecraft," *Journal of Guidance, Control, and Dynamics*, Vol. 31, No. 5, 2008, pp. 1478–1489. doi: 10.2514/1.29590.

[19] Y. Ariba, D. Arzelier, L. S. Urbina, and C. Louembet, "V-bar and R-bar Glideslope Guidance Algorithms for Fixed-Time Rendezvous: A Linear Programming Approach.," *Proceedings of the 20th IFAC Symposium on Automatic Control in Aerospace*, IFAC, 2016.